Thio-olivine Mn_2SiS_4 thin films by reactive magnetron sputtering: Structural and optical properties with insights from first principles calculations

A. Davydova[a], J. Eriksson[a], K. Rudisch[a], R. Chen[a], C. Persson[b,c], J. J.S.Scragg[a]

[a] *Ångström Solar Center, Solid State Electronics, Department of Engineering Sciences, Uppsala University, Box 534, SE-75121 Uppsala, Sweden*

[b]*Centre for Materials Science and Nanotechnology, Department of Physics, University of Oslo, P.O. Box 1048 Blindern, NO-0316, Oslo, Norway*

[c]*Department of Materials Science and Engineering, KTH Royal Institute of Technology, 10044, Sweden*

Abstract

Thio-olivines such as $(Fe,Mn)_2(Si,Ge)S_4$ have been proposed as candidate earth-abundant materials for single and multi-junction solar cells. In this work we present the first investigation of Mn_2SiS_4thin films prepared by reactive magnetron sputtering deposition, using a composition grading approach. Precursor instability in ambient conditions is observed, revealing the oxidation/hydrolysis of Si-S bonds from the as-deposited film as a blocking mechanism for the ternary compound formation. Structural, morphological and optical properties of the annealed Mn_2SiS_4 films are reported for the first time. Resulting Mn_2SiS_4 films have orthorhombic *Pnma* structure and are polycrystalline. Raman active modes at 325 nm excitation are observed at 262, 320, 400 and 464 cm^{-1}. From room temperature photoluminescence at 532 nm excitation the band gap is estimated to be about 1.9 eV, but a high optical absorption coefficient of > 10^4 cm^{-1} was only obtained at E > 2.8 eV. First principles calculations are used for better understanding of opto-electronic properties. From the calculations, Mn_2SiS_4 is suggested to have a band gap of about 1.73 - 1.86 eV depending on the magnetic configuration of Mn and slight indirect nature. The slow absorption onset is interpreted by strong anisotropy due to one of the components of the dielectric function.

Keywords: Magnetron sputtering deposition, Compositional grading, Thio-olivines, Thin films, Mn_2SiS_4

Highlights:

- for the first time, thin films manufacturing of thio-olivine material Mn_2SiS_4 is performed
- precursor instability is noted due to a highly reactive SiS_2 sub-phase formed during the deposition step
- absorption coefficient rise to 10^4 cm^{-1} 0.9 eV above the estimated band gap which is about 1.9 eV
- Mn_2SiS_4 films are suspected to be unsuited to photovoltaic applications despite theoretical predictions

1. Introduction

Recent activities in solar photovoltaics (PV) research focus on the demand of manufacturing new "absorber layer" materials, which are essential components in solar cell structures. There are a few requirements applied to these photo-active layers. Besides appropriate opto-electronic properties, it is nowadays important to consider earth-abundance, embodied energy, cost-effectiveness, low toxicity and long-term stability. Moreover, suitable materials with band gaps of about 1.6 – 1.8 eV are sought for producing next generation, multi-junction solar cells[1]. In order to fulfill these needs, researchers have broadened their search away from traditional solar cell materials such as crystalline Si, Cu(In, Ga)Se_2 and CdTe towards alternative, earth-abundant materials. It can require a considerable investment to develop a successful synthesis of a new material with sufficient quality to provide final conclusions on its suitability for PV. To assist in the search for new compounds, guidance from computational predictions can be extremely valuable too. Basic information that can be calculated for a prospective PV material includes the size and nature of the fundamental band gap and the magnitude of the absorption coefficient, but, as our computational abilities improve, it is natural to shift more of the burden of screening and evaluation of new compounds into the computational domain. In this work, we use experimental and theoretical approaches to study a new group of compounds recently predicted to have merit for PV. We find implications for both their practical application as well as for PV materials design efforts in the future.

Group of the compounds which is poorly investigated but might be promising for future PV technologies - the ternary metal chalcogenides with olivine structure. These compounds are related to the mineral "olivine" or magnesium iron silicate $(Mg, Fe)_2SiO_4$, which has an orthorhombic crystal structure and can be extensively found in the Earth's mantle. Earth-abundant metal chalcogenides with chemical formula $M_2T(S, Se)_4$, where M = Mg, Mn, Fe and T = Si, Sn, also exhibit the olivine structure, but are less studied in comparison with the namesake oxides.

Two specific thio-olivine materials reported in recent studies are the iron containing sulfides Fe_2SiS_4 (FSS) and Fe_2GeS_4 (FGS). Yu et al. [2] predicted both these compounds to be suitable for the absorber layer in solar cell structures and estimated band gap values of 1.40 – 1.55 eV (for the Ge and Si containing compounds respectively) and high

absorption coefficients > 10^5 cm^{-1}, by using density-functional theory calculations. Both FSS and FGS were prepared by Vincent et al. [3] as a single crystal and reported to have orthorhombic symmetry with *Pnma* space group. Baron et al. [4] provided neutron powder diffraction investigations of the structural and magnetic properties of Fe_2SiS_4. After the recent theoretical prediction [2], several experimental papers reported manufacturing of Fe_2GeS_4 colloidal nanostructures via solution synthesis [5] and solvent-free mechano-chemical processes [6]. The authors demonstrated XRD pattern of nanocrystals, as well as X-ray photoelectron spectroscopy and TEM imaging. Bo-In Park et al. [6] also provided diffuse reflectance spectra and room temperature photoluminescence measurements and measured the band gap of FGS to be about 1.41 - 1.43 eV which is quite similar to the predicted values from Yu et al. [2]. FGS nanoparticles reported to be rather stable after the synthesis [5, 6]. No thin film synthesis for FSS or device manufacturing for both FSS and FGS compounds was performed so far. However, a brief remark about the necessity to protect FSS precursors from oxygen contamination during the synthesis was made by Vincent [3], due to hydrolysis of SiS_2 in ambient air.

In comparison with iron–based thio-olivines, the manganese-based compound Mn_2SiS_4 (MSS) is much less investigated. However, as well as containing only earth-abundant elements, Mn-based thio-olivines have the same crystal structure and therefore are expected to have comparable optical properties, including a high absorption and a band gap suitable for solar cell structures. In particular, the band gap is expected to be somewhat larger than FSS and FGS, due to the smaller unit cell, which would be interesting for multi-junction solar cells. Due to magnetic nature of Mn, the MSS compound was primary investigated for its magnetic properties [7-10]. Fuhrmann and Pickard in 1989 reported MSS single crystal growth by using I_2 transport with MnS, Si and S_8 as reactants in sealed quartz ampoules at around 900K. As a result, an olivine structured crystal with *Pnma* group was investigated by XRD measurements – the first report about this compound [11]. Church et al. prepared a MSS single crystal for magnetic property investigations [10]. For $(Mn,Fe)_2SiS_4$, no thin film synthesis or optical property investigations were performed so far. However, if we propose the integration of Fe- or Mn- based thio-olivines in thin film solar cells, it is highly important to develop a thin film synthesis. Moreover, the demand of extensive experimental information

about optical and structural properties of FSS or MSS films should be fulfilled prior to any promises about PV applications.

In this work, we aim to shed light on one of the less investigated olivine structured compounds, Mn_2SiS_4, in thin-film form. Synthesis is made via magnetron sputtering deposition of precursors, followed by thermal treatment. A compositional grading approach helps to identify the chemical origin of instabilities of the precursor. Crystalline structure, morphology, Raman spectroscopy and optical properties are acquired for Mn_2SiS_4 thin films for the first time. In the last section we present analysis of the electronic and optical properties by *ab-initio* calculations which are of great help for understanding of the unusual optoelectronic properties of Mn_2SiS_4, and the potential role of thio-olivine compounds in PV applications.

2. Experimental

2.1 Synthesis and characterization

Thin film preparation with compositional variation across the sample was done by magnetron sputtering deposition in Von Ardenne CS 600 chamber. Pure Mn (99.95% purity, Kurt J. Lesker) and Si targets (99.9999% purity Si, undoped, Kurt J. Lesker) were connected to DC and RF sources respectively and reactively co-sputtered in H_2S + Ar atmosphere. The base pressure of the system was below $1 \cdot 10^{-6}$ mbar. A working pressure of $2 \cdot 10^{-2}$ mbar was reached by introducing H_2S and Ar mixture in the chamber with 1:1 ratio and mass flow rate of 25 sccm for both sources giving the total mass flow of 50 sccm. Co-sputtering was performed with power set to 200W and 250W on the Si and Mn target respectively. The substrate was heated to 300°C and the rotation of the substrate holder was switched off to create compositionally graded films with variation in stoichiometry from Si to Mn-rich sides. Before the actual thin film deposition, pre-sputtering of Mn and Si targets was done in Ar atmosphere for 20 minutes. Film thicknesses of 500 nm and 1500 nm were produced with sputtering time of 1.5 and 4 h respectively. In all cases, deposition was performed on both soda lime glass (SLG) and molybdenum-coated soda lime glass substrates with size of 50×10 mm^2 for 500 nm and 70×15 mm^2 for 1500 nm films respectively.

The resulting precursors were then directly transferred from the sputtering chamber to a tube furnace for the following annealing procedure. For annealing, as-deposited films were located in coated graphite box together with 14 mg of elemental sulphur (99.999% Alfa Aesar). The tube furnace was filled with static argon pressure of 350 Torrand pre-heated to a set temperature of 640°C. The graphite box was then inserted into the heated zone and left there for 10 minutes. The estimated sample temperature, from a thermocouple embedded in the sample holder, rose quickly to around 600°C during this process. The annealed samples then were moved to a cold zone and consequently cooled down to room temperature within 40 minutes.

Compositional analysis of the precursors and annealed Mn_2SiS_4 films was performed by energy dispersive X-ray spectroscopy (EDS) by Zeiss Leo 1550 electron microscope and morphology of the films were examined by scanning electron microscope (SEM) on the same instrument. EDS data was collected at 12 keV accelerating voltage and Mn/Si, S/(2Si+Mn) and O/(Si+Mn+S) ratios were quantified statistically across the graded film surface. From chemical formula of Mn_2SiS_4 compound, the Mn/Si ratio should be equal 2 at stoichiometric composition and vary elsewhere on the graded sample. The S/(2Si+Mn) should always be 1 if Mn and Si are in their II and IV oxidation states, respectively. No significant amount of O is expected to arise in the film directly after the deposition or after the annealing processes.

Grazing incidence X-ray diffraction (GI-XRD) was done in a Philips MRD II system with Cu Kα radiation (λ = 1.5406 Å) with incident angle 1°.

Renishaw in Via system was used for Raman spectroscopy and room temperature photoluminescence (RT-PL) study by using excitation wavelengths of 325 nm, 532 nm and 785 nm respectively.

Transmission and reflection (R&T) spectra were recorded in a Bentham PVE300 system which features a Xenon and a Quartz-Halogen lamp as light sources and a movable integrating sphere with an entrance port of 5 - 15 mm in diameter (variable by apertures). For the analysis of the absorption characteristics, the absorption coefficient α was calculated with the following formula, where *d* is the thickness of the absorbing film, *R* the reflection and *T* the transmission[12]:

$$\alpha = \frac{1}{d}\ln\left(\frac{1-R}{T}\right).$$

2.2 Numerical methods for ab-initio calculations

The electronic and optical properties were theoretically investigated by means of the plane augmented wave (PAW) formalism within density functional theory (DFT) as implemented in the VASP program package [13, 14]. Modeling of a Mn_2SiS_4 crystal was performed with a 28-atom cell with an antiferromagnetic phase, with crystalline space group *Pnma* (D_{2h}^{16}; group number 62). The calculated properties are described with an exchange-correlation potential within the Perdew-Burke-Ernzerhof (PBE) [15] generalized gradient approximation (GGA) exchange-correlation functional revised for solids (PBEsol) [16] and on site Coulomb interaction correction[17] of the *d*-like orbitals for magnetic atoms (i.e., PBEsol+*U*). Our previous studies showed that it is crucial to take into account the U_d parameter in order to determine the magnetic configuration and lattice parameters accurately [2, 18, 19]. Here, U_d(Mn) = 4.0 eV is chosen according to Setyawan *et al*. [20]. This way the *d*-like states are corrected, and the band gap is widened by more than 1.0 eV. The crystalline structures were fully relaxed until the total energy and the residual force on each atom showed convergence within 0.1 and 10 meV/Å, respectively. The fully relaxed lattice constants were a = 12.627 Å, b = 7.384 and c = 5.907 Å. All the electronic and optical calculations with spin polarization were performed utilizing PBEsol+*U* with an energy cutoff of 400 eV and k-mesh of 4×6×8.

3. Results and discussion

3.1 Investigation of the Mn_2SiS_4 precursor stability

Since there are no reports about manufacturing of Mn_2SiS_4 thin films, our deposition conditions were chosen based on several empirical attempts. First, we tested two-step process with the metallic stacking of Mn and Si at different substrate temperatures and subsequent sulfurization. This led to the formation of a MnSi alloy in the precursor and formation of the admixtures of MnSi and MnS phases after the sulfurization step. The resulting thin films were semi-transparent and dark-brown with an opaque layer on top. It was concluded that insufficient sulfur incorporation into the MnSi alloy was occurring in the sulfurization step due to poor reactivity of silicon towards sulfur (as noted also for

Fe_2SiS_4[21]). Thus, the two-step approach with reactive co-sputtering was used as discussed in the experimental section. The resulting graded Mn-Si-S precursors looked uniform, yellowish, transparent and reflective, but released a strong H_2S odor. Further observation of the as-grown films in ambient atmosphere showed that the reflective appearance was lost within several days - a clear indication of spontaneous oxidation of the Mn-Si-S precursor.

Since MSS itself is known to be a stable compound [7-11], our assumption was that the reactively sputtered precursor did not contain only MSS itself, but instead/also sub-phases such as MnS and SiS_2 were formed during the deposition process. If this was the case, then the highly reactive SiS_2 would hydrolyze rapidly in the air with release of volatile H_2S products. Thus, undesirable $Si(OS)_x$, $Si(OH)_x$ or SiO_2 groups might form instead and replace SiS_2[22, 23]. Since silicon has strong binding with oxygen, hydroxyl or oxy-sulfide groups, this would prevent sulfur replacing them during the sulfurization process.

To address this issue, an additional investigation of the Mn_2SiS_4 precursor stability was performed. Three graded Mn_2SiS_4 precursors *N1, N2* and *N3* with 500nm thickness were deposited on Mo coated SLG and then each of them underwent different treatment paths. The composition of precursor *N1* was measured by EDS across the Mn to Si-rich stoichiometry in 4 respective areas (see Figure 1a). Mn/Si, S/(2Si+Mn) and O/(Mn+Si+S) ratios were then quantified based on the EDS. Compositional measurements were done on the as-grown precursor *N1* first and then after two and seven days of sample exposure to the ambient atmosphere. Each time, EDS measurements were conducted at the same locations. The as deposited precursor *N2 (non-oxidized precursor)* was transferred directly from the sputtering chamber to the vacuum storage and sample *N3 (oxidized precursor)* was exposed to the air for three days. Then, both precursors *N2* and *N3* underwent the annealing process as described in the experimental section. After the heat treatment, both films *N2* (annealed from a *non-oxidized precursor*) and *N3 (*annealed from an *oxidized precursor)* were analyzed by GI-XRD.

Figure 1c shows results of the EDS study on MSS precursor *N1* where S/(2Si+Mn) and O/(Si+Mn+S) are plotted separately as a function of Mn/Si ratio. The Mn/Si content did not change during the 7 days. However, sulfur and oxygen contents were changed with time and showed strong dependence on composition variation. Initially, precursor *N1* had no presence of oxygen and contained sufficient amount of sulfur across the whole

area, so that the S/(2Si+Mn) ratio was about 1.37-1.35 in all four measured areas (thus somewhat over-stoichiometric in S). However, between 2 -7 days of air exposure, losses of S were correlated with O-enrichment on the Si-rich side (Mn/Si < 1.6) so that the S/(2Si+Mn) ratio went down to 0.8 and the O/(Si+Mn+S) ratio went up to 0.7. This S-O exchange was observed less extensively on the Mn-rich side (Mn/Si > 1.8) where the S/(2Si+Mn) ratio decreased to 1.1, while the O/(Si+Mn+S) ratio increased only up to 0.2. Since the Si-rich side of the sample appears to be most susceptible to oxidation, we conclude that the reactively sputtered precursors suffered from oxidation/hydrolysis of Si-S bonds upon air exposure. However, it appears that fast transfer of the precursor from the sputter chamber to the anneal system (a similar air exposure time as for the first set of measurements on *N1*) can avoid this problem to a large extent.

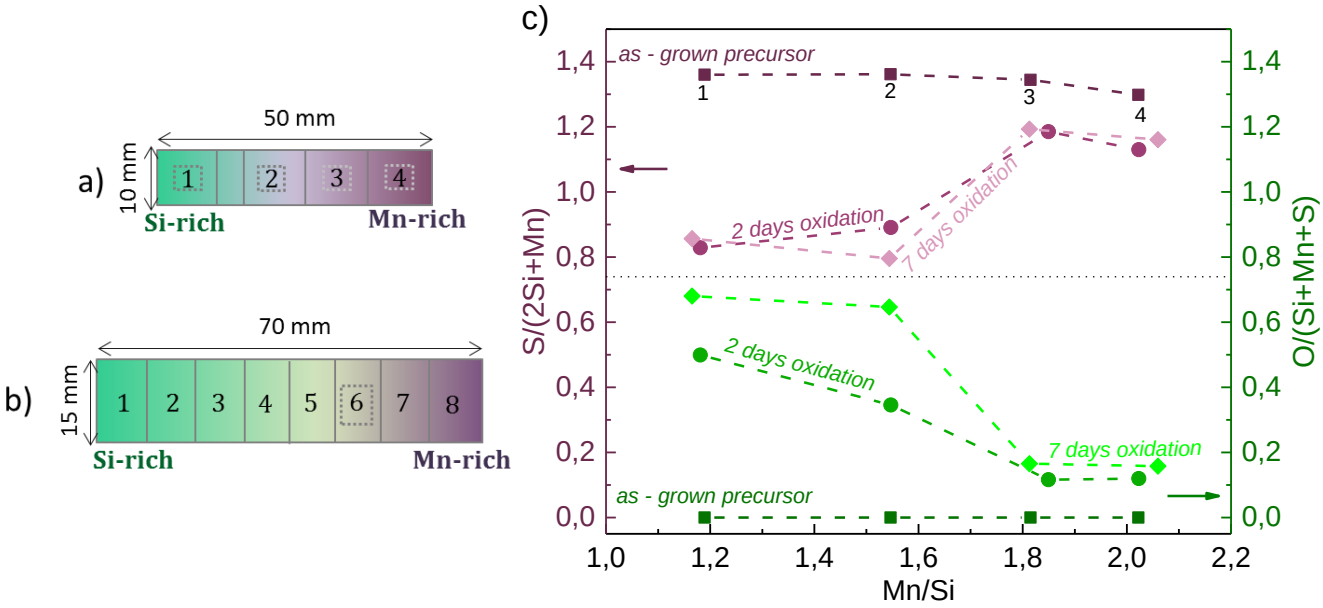

Figure1. Schematic representation of samples corresponding to film thicknesses of 500 nm (a) and 1500 nm (b) respectively. Fields 1-4 and 1-8 schematically show regions where EDS and other measurements were conducted. (c) EDS measurements across the compositional gradient of the precursor *N1,* where S/(2Si+Mn) (violet) and O/(S+Mn+Si) (green) are plotted as a function of Mn/Si ratio on as grown film and after 2 and 7 days of oxidation in the ambient atmosphere. Measurements were conducted on respective fields 1-4 as depicted on Figure 1a.

The composition variation in the precursors *N2* and *N3* was very similar to that obtained in *N1* since they were made at the same deposition round. Thus, precursor *N3* after three days of the air exposure had sulfur loss and oxygen enrichment across the compositional gradient, similar to *N1*, while *N2* was keeping the initial sulfur-rich

composition and absence of oxygen content, having been stored in vacuum. After the annealing process, both *non-oxidized precursor after anneal* (*N2*) and *oxidized precursor after anneal* (*N3*) were analyzed by X-ray diffraction. In order to simplify data representation in Figure 2, we show the resulting GI-XRD patterns only on extreme points of Si and Mn rich sides where Mn/Si ≈ 1.3 and 2 respectively (which correspond to point 1 and 4 depicted in Figure 1a).

From the XRD study of the film *N2* (Figure 2 a, b) only a MnS phase (denoted by **+**) was found on both sides of the graded film and the peak denoted by (*****) corresponds to Molybdenum. A stronger contribution from MnS was found on the Mn-rich side. In contrast, multiple peaks on both Mn and Si-rich sides were found on the film *N3* (Figure 2 c, d). The obtained XRD data corresponded to the orthorhombic structure of Mn_2SiS_4 (denoted by ¤). On the Mn-rich side where Mn/Si ≈ 2 an additional contribution from MnS phase was found. The XRD results of the annealed films *N2* and *N3* clearly exhibited the negative effect of the oxidation process on the formation of Mn_2SiS_4 phase. From stoichiometric point of view, XRD also showed that thin film structure where Mn/Si ratio equal 2 and higher is accompanied by MnS secondary phase, while it is not seen in silicon rich part of the film where Mn/Si < 1.5.

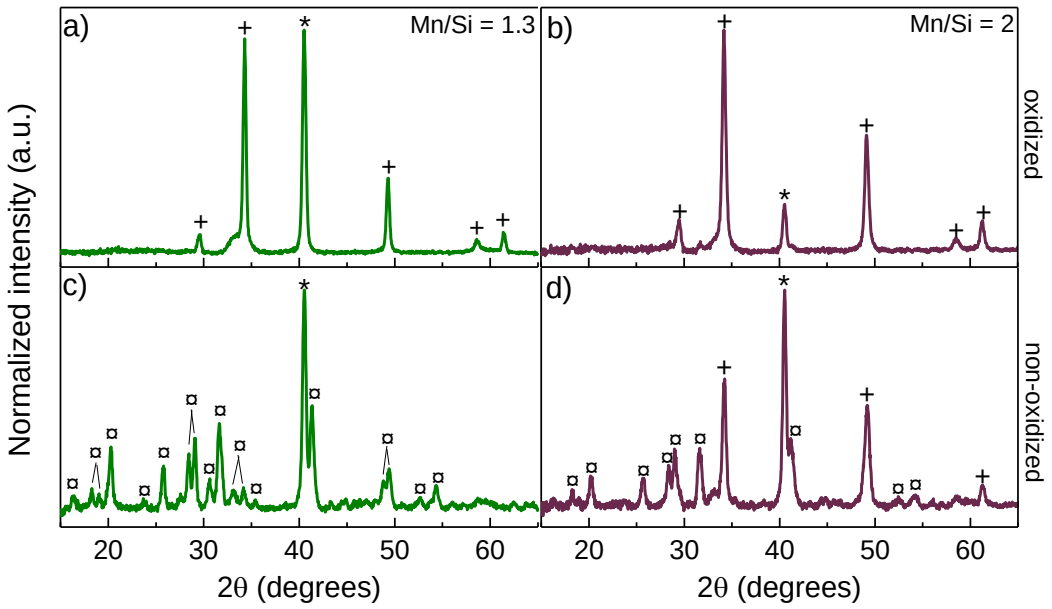

Figure 2. (a, b)GI-XRD pattern of the samples annealed from an oxidized precursor *N2* and (c, d) annealed from a non-oxidized precursor *N3*. Peaks related to MnS phase denoted by (+) and Mo peak is indicated as (*). XRD pattern of Mn_2SiS_4 structure is shown by (¤).

3.2 Structural and optical properties of Mn_2SiS_4

Taking into account that the Mn_2SiS_4 precursors were found to be unstable in the ambient atmosphere and a MnS secondary phase was appearing on Mn-rich side, we made one more deposition of the thicker films with broader stoichiometry range for investigation of structural and optical properties.

Co-sputtered compositionally graded Mn_2SiS_4 films with thickness of about 1500 nm were deposited on SLG and Mo coated SLG substrates with the size of 70×15 mm^2. The resulting precursors were immediately transferred from the deposition chamber to the annealing furnace. The annealed Mn_2SiS_4 thin film on SLG was used for optical measurements (reflectance, transmittance) and the films prepared on Mo coated SLG substrate were used for XRD, SEM, Raman spectroscopy and RT-PL analysis respectively. All the measurements were performed on the same locations along the compositional gradient. For simplicity, here we present only the data corresponding to the region between Mn and Si –rich sides where Mn/Si ratio is about 1.4 (the respective area is denoted as the field number 6 in Figure 1b). This way we would definitely avoid MnS secondary phases appearing on the film surface.

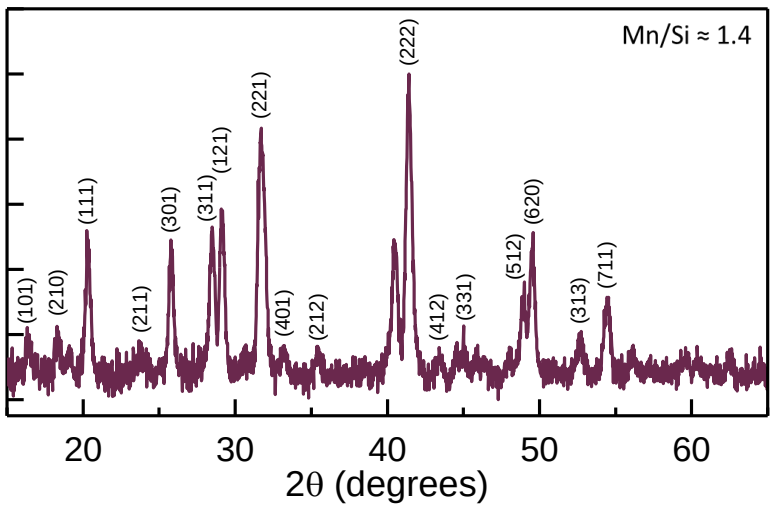

Figure 3. XRD pattern of Mn_2SiS_4thin film structure (PDF 04-007-7077) acquired on the annealed graded film in the region where Mn/Si ratio is about 1.4.

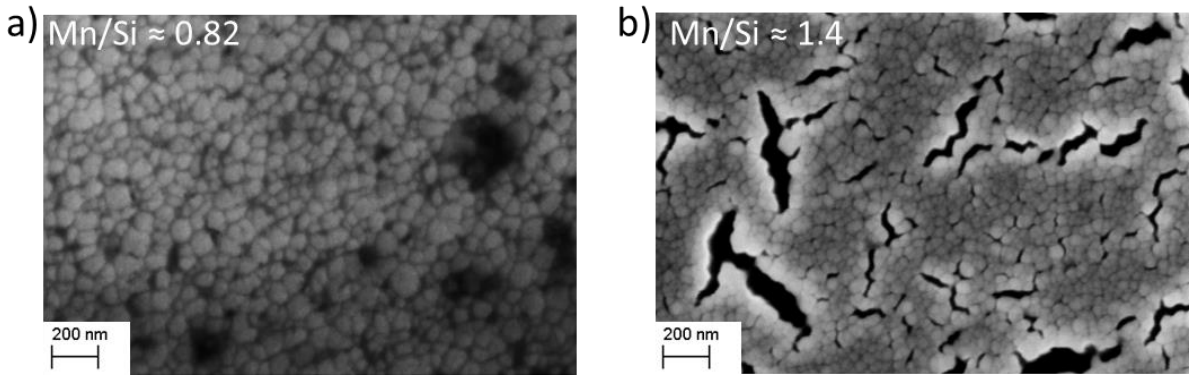

Figure 4. SEM images of the Mn_2SiS_4 graded film corresponding to regions where Mn/Si is about 0.82 (a) and 1.4 (b) respectively.

Obtained diffraction patterns along the graded sample correspond to orthorhombic *Pnma* structure (group number 62) with lattice parameters a = 12,688, b = 7,429 and c = 5,942 Å. An example of the XRD pattern for Mn/Si ≈ 1.4 is shown in Figure 3. The appearance of multiple peaks reveals an absence of preferential crystalline orientation and implies the expected polycrystalline structure. The peak at around 40.2° is assigned with Mo and well resolved along the graded sample due to the large surface area pinholes or cracks on the sample which could be seen by SEM analysis (Figure 4a, b). No sign of MnS phase is found on the investigated area of the graded film. A general observation after the XRD analysis is that the difference between diffraction patterns across the compositional gradient is small. In the area where Mn/Si > 1.4 XRD peaks are a bit more intense and well-resolved, which might suggest better quality of the film due to Mn-enriched stoichiometry. Contributions from secondary phases were not found on a chosen area of the graded sample but could be seen only on very Mn-rich side where Mn/Si ≥ 2, which is consistent with the results obtained in the precursor stability study.
Microscopy analysis along the compositional gradient showed a homogeneous film with well-resolved grains with the average size of 20-30nm. In the part of the film where the Mn/Si ratio varied between 1.2 and 2.2, small cracks on the surface could be seen across the area (Figure 4b). On Si-rich side where Mn/Si < 1.2 these cracks are not seen anymore, but pinhole-like areas appear along the surface (Figure 4a).

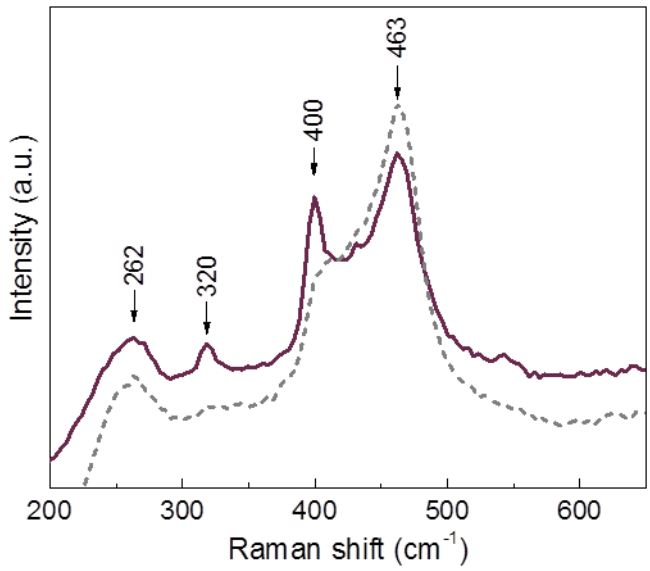

Figure 5. Raman spectra acquired at 325nm excitation wavelength corresponding to the Mn_2SiS_4 film measured in the region where Mn/Si ≈ 1.4 (Violet solid curve). The grey dotted curve shows the Raman spectrum measured on the same compositional region but a slightly different location.

Raman spectroscopy results obtained at 325nm excitation wavelength are shown in Figure 5. To our knowledge, no Raman data could be found for this compound in previous publications, so on the basis of the XRD observations we assumed that all obtained Raman peaks could be assigned to the polycrystalline orthorhombic *Pnma* structure of Mn_2SiS_4. The main peaks for Mn_2SiS_4 were found to be at 262, 320, 400 and 464 cm^{-1}. Spectra acquired on different sample areas from Mn- to Si-rich stoichiometry show similar trends. However, it was observed that some Raman modes are sensitive to spectrum acquisition conditions. Typically, well-resolved peaks at 320 cm^{-1} and 400 cm^{-1} could be seen in the beginning of the measurements but decreased in intensity during the data collection (grey curve in Figure 5). Simultaneously, the intensity of the peak at 463 cm^{-1} becomes stronger with the measurement time. The effect of diminishing some of the peaks on the spectrum can be explained by local heating of the sampling area under illumination by excitation laser, which probably led to a local phase transition or oxidation.

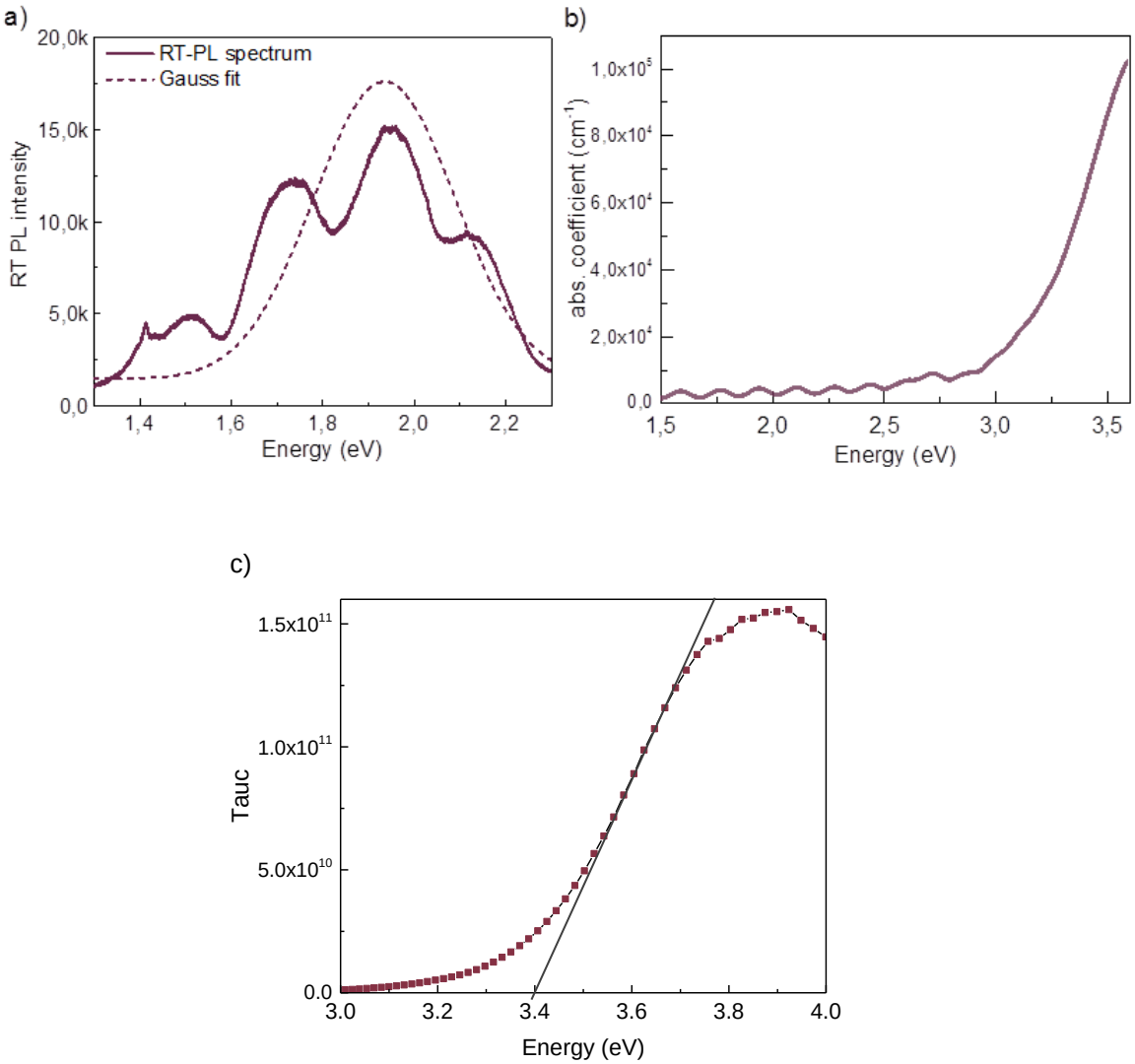

Figure 6. (a) RT-PL measurement results performed on Mn_2SiS_4 film in the region where Mn/Si ≈ 1.4 (solid). The dashed curve corresponds to a Gauss fit of the acquired spectrum. (b) Absorption coefficient of Mn_2SiS_4 film obtained from reflectance and transmittance measurements on the compositional region where Mn/Si ≈ 1.4. (c) Tauc plot for Mn_2SiS_4.

For RT-PL measurements the fluorescence spectra were obtained with a 532 nm excitation wavelength (Figure 6a). One can see that the acquired spectrum at Mn/Si = 1.4 contains interference fringes, but by using Gauss fit [24] we could estimate a broad PL maximum. Assuming that band-to-band transitions dominate at room temperature [6], we deduce the band gap value to be about 1.9 eV.

Transmission and reflection measurements were provided on the annealed MSS film deposited on SLG substrate and the absorption coefficient was calculated in the wavelength range of 300-1700 nm. A rather high optical absorption coefficient of about 10^5 cm^{-1} was found on both Mn- and Si-rich sides of the graded film (Figure 6b shows

results for Mn/Si ≈ 1.4). However, absorption becomes pronounced only at E>2.8 eV. An estimation of the band gap using a Tauc plot for a direct band gap material; see Fig. 6c) yields a value of about 3.4 eV, much larger than the band gap estimated from RT-PL at 1.9 eV. An indirect band gap at lower energy could account for this difference, but interference issues make analysis of the lower energy portion of the absorption spectrum impossible. Another explanation for the observed absorption edge could be the presence of MnS phases or oxide phases in the film (especially MnS with a direct band gap of 3.1-3.4 eV [25, 26] which coincides with the observed absorption edge). However, such strong absorption would necessitate a substantial amount of MnS, or oxygen in the film. The film was deliberately Mn-poor, and neither XRD nor Raman indicated any presence of MnS secondary phase (conversely, MnS can be seen for Mn-rich compositions). Regarding oxides, the oxygen content in the samples that were transferred directly from sputtering chamber to annealing furnace was minimal (so that O/(Mn+Si+S) ratio was about 0.01-0.02). Therefore, the only phase expected (and indeed, observed) in the films, namely Mn_2SiS_4, must be responsible for the observed absorption. The fact that the band gap estimate from the Tauc plot does not agree better with the band gap estimated from PL is puzzling. In order to understand better the optoelectronic properties of Mn_2SiS_4film, an additional theoretical investigation was conducted by *ab-initio* methods.

3.3 Optoelectronic properties calculation

The olivine structure of Mn_2SiS_4 compound corresponds to orthorhombic structure with a space group *Pnma* (see Figure 7a). The primitive cell used in calculations contained 8 Mn atoms, 4 Si atoms, and 16 S atoms. The Mn and S atoms form a distorted MnS_6 octahedron in two different Wyckoff positions, 4a and 4c [27]. The Mn-S bond length (δ_{Mn-S}) then is varied between 2.55 Å and 2.60 Å (2.58 Å average) at 4a sites, and between 2.53 Å and 2.62 Å (2.59 Å in average) at 4c sites. The averaged bond length at 4c sites is slightly larger than the one at 4a sites, and similar observation was made for Fe_2GeS_4 olivine structure in [27].

From the calculated electronic band structure shown in Figure 7b, the fundamental band gap (E_g) of Mn_2SiS_4 has an indirect nature. The maximum of the topmost valence band

(VB) occurs on the Γ-point while the minimum of lowest conduction band (CB) occurs on the symmetry line between the Γ- and Z-points.

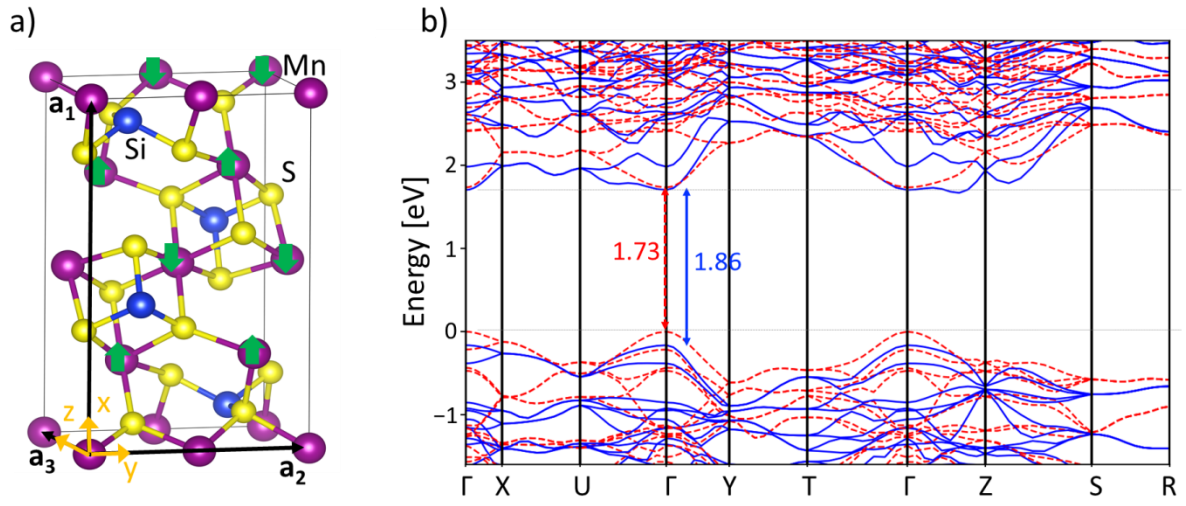

Figure 7. (a) Schematic representation of the Mn_2SiS_4 crystal structure. The primitive cell of the crystal is defined by the lattice vectors $\mathbf{a_1}$, $\mathbf{a_2}$, and $\mathbf{a_3}$, and the orientation of the polarization is described by the Cartesian coordinate **x**, **y**, and **z**. The calculated antiferromagnetic configuration is indicated by the green arrows. (b)The electronic band structure of Mn_2SiS_4. The spin-up and spin-down like states are represented by the red-dashed and blue-solid lines.

The minimal direct gap energies from the calculated band structure for spin-up and spin-down are 1.73 and 1.86 eV respectively. The difference between the indirect gap energy and minimal direct gap energy is only about 40 meV in both spin-alignment cases, which generally indicates the lowest CB to be flat. However, for this material, the lowest CB is not homogeneously flat, especially along the Y- and T-points. The band structure has not the feature of multi-valley with flat energy dispersions [28], hence, the absorption is not apparently enhanced. The hybrid functional approach such as HSE06 generally is believed to predict better the band gap value. However, from the test calculations of Fe_2SiS_4, which has the same crystal structure and also contains magnetic element as in Mn_2SiS_4 case, the calculated band gap value is around 1.50 eV and 2.35 eV by utilizing PBEsol+*U* and HSE06, respectively. Since the measured band gap for Fe_2SiS_4 is found to be about 1.54 eV [2], we can assume that PBEsol+*U* generates a more reasonable band gap energy than HSE06 for this type of material. The states nearby the first VB for Mn_2SiS_4 are mainly Mn *d*-like and S *p*-like states, however, nearby the lowest

CB, they mainly contain Mn *d*-like, as well as slight Si *s*-like states (not shown). The states in Mn_2SiS_4 are similar as Fe_2SiS_4 (Fe *d*-like states instead of Mn *d*-like states) in [2]. The prediction of the band gap value from DFT calculations is then relatively close to the experimental band gap estimated in this study by RT-PL, but does not match the estimate from the absorption coefficient of about 3.3 eV seen in optical R&T measurements.

In the following study, tensor$\varepsilon_2(\omega)$ with components α and β (i.e., $\varepsilon_{2,\alpha\beta}$ (ω)) was first calculated within the linear response of optical transition probability between occupied and unoccupied states, then $\varepsilon_{1,\alpha\beta}$ (ω) was obtained via the Kramers-Kronig transformation utilizing $\varepsilon_{2,\alpha\beta}$ (ω) [13, 14]. The absorption coefficient $\alpha(\omega) = \omega c^{-1}(2|\varepsilon(\omega)| - 2\varepsilon_1(\omega))^{1/2}$ was then determined directly from the complex dielectric function $\varepsilon(\omega) = \varepsilon_1(\omega) + i\varepsilon_2(\omega)$, where c is the speed of light.

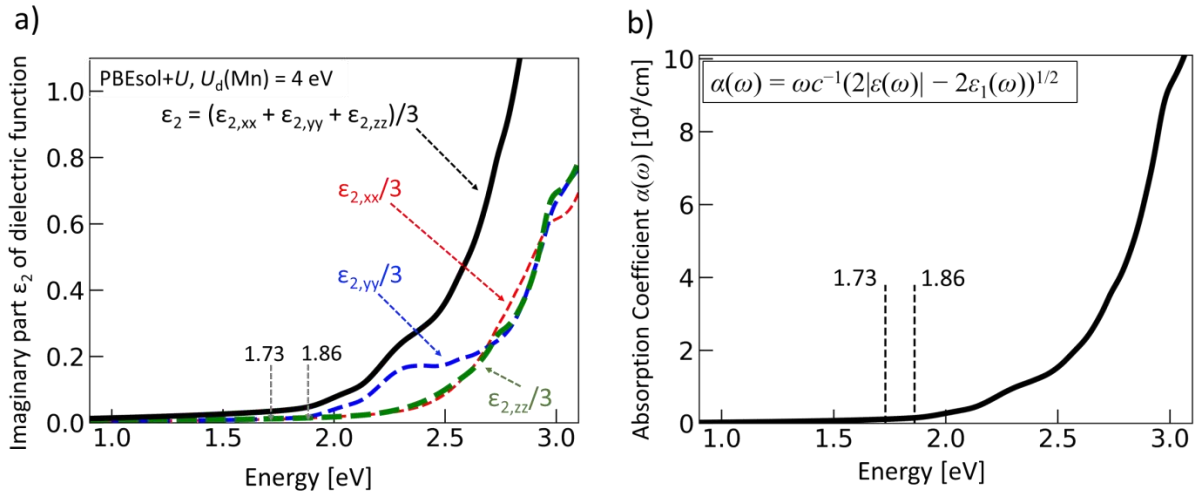

Figure 8. (a) Polarization dependency of the dielectric function of Mn_2SiS_4 calculated by the PBEsol+*U* method. The calculated dielectric response ε_2 is rather anisotropic between E_g and E_g + 0.75 eV. The minimum of direct gap energy for spin-up or spin-down is 1.73 and 1.86 eV, respectively. (b) Calculated absorption coefficient of Mn_2SiS_4.

Figure 8a demonstrates weak response in the calculated dielectric function (ε_2) which is observed nearby the E_g, which remains up to around E_g + 0.5 eV. This weak response is not expected, but from the test calculations, we confirm that this effect did not appear due to the sparse **k**-mesh in the calculation as indicated in [29], but rather appears to be characteristic of Mn_2SiS_4.As demonstrated further in Figure 8a, the components ($\varepsilon_{2,xx}$,$\varepsilon_{2,yy}$, and $\varepsilon_{2,zz}$) of the calculated dielectric function are very anisotropic in the region

nearby E_g. The polarization in the y-direction is dominating between around E_g and E_g + 0.75 eV which explains partially, but not completely, the weaker absorption nearby the E_g (Figure 8). It shows that Mn_2SiS_4 exhibits a rather weak absorption nearby the E_g estimated by band structure (1.73 – 1.86 eV), which is most likely due to the weak response in dielectric function components. However, a strong absorption is observed from around E_g + 0.75eV.

3.4 Discussion and remarks

By comparing experimental and theoretical data for the studied material one can find certain qualitative agreement in optoelectronic properties particularly in the "exponential" shape of the absorption coefficient spectrum. The estimated band gaps from electronic band structure (1.73 and 1.86 eV for spin-up and spin-down configurations) and photoluminescence measurements (~1.9 eV) are also in relatively good agreement within expected errors relating to the choice of the potential and complexity in the description of semiconducting properties for materials which contain magnetic atoms such as Mn. Unusually for a direct band gap material, the observed onset of optical absorption is much delayed compared with the band gap value estimated above. This might suggest the appearance of a possible forbidden transition between bands. Although at present the origin of the delayed absorption onset is not completely clear, we conclude based on the agreement between the PL and the calculations that the "true" electronic band gap of Mn_2SiS_4 is around 1.9 eV, and that the band gap estimate obtained directly from the optical measurements (~3.3 eV) is simply an artifact of delayed optical absorption.

The electronic band gap of Mn_2SiS_4, determined here for the first time to be ca. 1.9 eV, is in principle suitable for an upper cell in a multi-junction solar cell [1]. However, the absorption characteristics of this material unfortunately make it unsuitable for this application. Despite the reasonable electronic band gap, Mn_2SiS_4 has very weak light absorption until photon energies above 3 eV, and therefore a very thick layer of material would be needed to capture a substantial portion of incoming light with energy above the electronic band gap. The strong absorption of higher energy photons is of no benefit, since the thus photo-excited electrons will quickly thermalize to the electronic band gap, losing a large fraction of their energy. An interesting anisotropy of the dielectric

function was determined from calculations, with the $\varepsilon_{2,yy}$ component being somewhat stronger, suggesting that appropriate control of crystallographic orientation could potentially improve the measured absorption coefficient (whereas the samples prepared here were polycrystalline without strong preferred orientation). However, the gain from this would be relatively small. Therefore, potential use of Mn_2SiS_4 films in the PV applications (thin film solar cells in particular) is rather doubtful.

Regarding future materials prediction studies for PV, we suggest that an important screening criterion, besides simply a "high" absorption coefficient ($\alpha > 10^4$ cm^{-1}), should be an absorption coefficient that rises rapidly above the electronic band gap. This screening criterion can be easily applied, and a rule of thumb based on current direct band gap solar absorbers such as $CuInSe_2$, InP, GaAs is that the absorption coefficient should rise to 10^4 cm^{-1} within around 150 meV of the electronic band gap. By that metric, even the other thio-olivine compounds recently proposed for PV applications, Fe_2SiS_4 and Fe_2GeS_4, compare rather poorly: their absorption coefficients only rise to 10^4 cm^{-1} 0.65 and 0.5 eV above their respective band gaps [2]. The result is that thicker layers of these new materials would be needed compared to existing materials. This raises the question of whether the thio-olivines as a material group are fundamentally unsuitable for PV applications, despite the initial promises.

A more general remark about materials design concerns the chemical stability of new compounds predicted by theoretical calculations. Both Fe_2SiS_4 and Fe_2GeS_4 were calculated to be stable ternary compounds on the basis that the following hypothetical formation reactions have negative free energy changes [2]:

$$2\ FeS + SiS_2 \rightarrow Fe_2SiS_4$$

$$2\ FeS + GeS_2 \rightarrow Fe_2GeS_4$$

However, this is far from a sufficient criterion, because if materials are to be synthesized and used in applications, they should ideally be able to tolerate ambient conditions, i.e. air and at least traces of moisture. To get a rough picture of the stability of an unknown material in ambient conditions, we suggest looking at the stability of the respective "equivalent binary" compounds with the same oxidation states [30], in the above cases FeS, SiS_2 and GeS_2. In most cases, this will already be well-known from experimental work. In the above examples, and the case of Mn_2SiS_4, the relevant equivalent binaries

are FeS, SiS_2, GeS_2 and MnS. FeS, GeS_2 and MnS are rather stable, but it is known that SiS_2 hydrolyzes in the air. This does not automatically mean that Fe_2SiS_4 and Mn_2SiS_4 will also undergo hydrolysis once successfully grown, but it does raise warnings about possible difficulties with synthesis; indeed, the oxidation of Mn_2SiS_4 precursors encountered in this work and similar reported issues for Fe_2SiS_4 seem to stem from the instability of SiS_2 [3, 31]. Exchanging Si for Ge, as in Fe_2GeS_4, the equivalent binaries are now all rather stable, and indeed there are no discussions about synthesis problems with the Ge-containing compounds in the literature so far [2, 5, 6, 32]. Therefore, in the future it is suggested to develop predictions of material "stability" a little further, and one approach to do this is to consider not only the stability of the final desired structure but also of the possible equivalent binaries.

4. Conclusions

In this work we report deposition of olivine structured Mn_2SiS_4 thin films. Thio-olivines such as Mn_2SiS_4 have been earlier proposed from theoretical studies to have potential in photovoltaic (PV) applications. We use a two-step process of reactive magnetron sputtering and subsequent sulfurization at high temperature. The stability of the compositionally graded Mn-Si-S precursors was investigated first, and it was found that sulfur-oxygen exchange took place extensively on the Si-rich side through hydrolysis of SiS_2 in the ambient atmosphere, which presented a blocking mechanism for Mn_2SiS_4 compound formation. Thus, avoiding oxidation of the precursor was suggested as an important issue for compound manufacturing through the chosen synthesis route. In general, precursor stability is noted to be an important issue for Si-based ternary sulfide compounds such as Mn_2SiS_4 and Fe_2SiS_4. Successfully deposited Mn_2SiS_4 thin films showed good agreement in structural properties with previously obtained results from single crystal manufacturing. Raman spectroscopy and room temperature photoluminescence analysis together with optical characterization by reflectance and transmittance measurements were acquired for the first time for this particular material. Electronic structure, absorption coefficient and dielectric function calculations by *ab-initio* methods were also conducted in this study and provided support in understanding the unusual optoelectronic properties of the investigated material, which has a strongly delayed onset of optical absorption above the electronic band gap. By the

combined experimental and theoretical approaches, we could conclude that Mn_2SiS_4 is unsuitable for PV applications due to a combination of relatively poor chemical stability of the precursor and unfavorable absorption characteristics of the resulted thin film, properties which seem to be shared with other members of this material group. Finally, we make some suggestions for future PV "materials design" exercises that could help to screen out materials with similar optical and stability issues before they are put forward for experimental development.

5. Acknowledgements

The authors acknowledge funding by the Swedish Energy Agency, the Swedish Research Council and the Swedish strategic research program StandUp for Energy. R. Chen and C. Persson acknowledge support from Research Council of Norway (project 243642) and access to high-performance computing resources via SNIC and NOTUR. A. Davydova thanks Christopher Frisk and Fredrik Larsson for the assistance in R&T and XRD measurements.

6. References

[1] S.P. Bremner, C. Yi, I. Almansouri, A. Ho-Baillie, M.A. Green, Optimum band gap combinations to make best use of new photovoltaic materials, Solar Energy, 135 (2016) 750-757.
[2] L. Yu, S. Lany, R. Kykyneshi, V. Jieratum, R. Ravichandran, B. Pelatt, E. Altschul, H.A.S. Platt, J.F. Wager, D.A. Keszler, A. Zunger, Iron Chalcogenide Photovoltaic Absorbers, Advanced Energy Materials, 1 (2011) 748-753.
[3] H. Vincent, E.F. Bertaut, W.H. Baur, R.D. Shannon, Polyhedral deformations in olivine-type compounds and the crystal structure of Fe2SiS4 and Fe2GeS4, Acta Crystallographica Section B, 32 (1976) 1749-1755.
[4] V. Baron, Ö. Amcoff, T. Ericsson, Neutron powder diffraction study of the crystal and magnetic structures of Fe2SiS4, Journal of Magnetism and Magnetic Materials, 195 (1999) 81-92.
[5] S.J. Fredrick, A.L. Prieto, Solution Synthesis and Reactivity of Colloidal Fe2GeS4: A Potential Candidate for Earth Abundant, Nanostructured Photovoltaics, Journal of the American Chemical Society, 135 (2013) 18256-18259.
[6] B.-I. Park, S. Yu, Y. Hwang, S.-H. Cho, J.-S. Lee, C. Park, D.-K. Lee, S.Y. Lee, Highly crystalline Fe2GeS4 nanocrystals: green synthesis and their structural and optical characterization, Journal of Materials Chemistry A, 3 (2015) 2265-2270.

[7] A. Junod, K.Q. Wang, G. Triscone, G. Lamarche, Specific-Heat, Magnetic-Properties and Critical-Behavior of Mn2sis4 and Fe2ges4, Journal of Magnetism and Magnetic Materials, 146 (1995) 21-29.
[8] K. Ohgushi, Y. Ueda, Spin-flop multicritical phenomena in Mn2AS4(A=Si and Ge), Journal of Magnetism and Magnetic Materials, 310 (2007) 1291-1292.
[9] J.H. Chung, K. Ohgushi, Y. Ueda, Magnetic phase diagrams of the multicritical olivine Mn2SiS4 and Mn2GeS4, Journal of Magnetism and Magnetic Materials, 322 (2010) 832-837.
[10] C.J. Church, The structural, thermal and magnetic properties of Mn2SiS4, Department of Physics, University of Ottawa, Ottawa, Canada, 1994.
[11] J. Fuhrmann, J. Pickardt, Structure of Mn2SiS4, Acta Crystallographica Section C, 45 (1989) 1808-1809.
[12] H. Wu Qu, Extraction of extinction coefficient of weak absorbing thin films from special absorption, Journal of Physics D: Applied Physics, 22 (1989) 1384.
[13] G. Kresse, J. Furthmüller, Efficient iterative schemes for ab initio total-energy calculations using a plane-wave basis set, Physical Review B, 54 (1996) 11169-11186.
[14] G. Kresse, D. Joubert, From ultrasoft pseudopotentials to the projector augmented-wave method, Physical Review B, 59 (1999) 1758-1775.
[15] J.P. Perdew, K. Burke, M. Ernzerhof, Generalized Gradient Approximation Made Simple, Physical Review Letters, 77 (1996) 3865-3868.
[16] J.P. Perdew, A. Ruzsinszky, G.I. Csonka, O.A. Vydrov, G.E. Scuseria, L.A. Constantin, X. Zhou, K. Burke, Restoring the Density-Gradient Expansion for Exchange in Solids and Surfaces, Physical Review Letters, 100 (2008) 136406.
[17] V.I. Anisimov, J. Zaanen, O.K. Andersen, Band theory and Mott insulators: Hubbard U instead of Stoner I, Physical Review B, 44 (1991) 943-954.
[18] C.E. Cava, C. Persson, A.J.G. Zarbin, L.S. Roman, Resistive switching in iron-oxide-filled carbon nanotubes, Nanoscale, 6 (2014) 378-384.
[19] R. Chen, C. Persson, Electronic and optical properties of Cu2XSnS4 (X = Be, Mg, Ca, Mn, Fe, and Ni) and the impact of native defect pairs, Journal of Applied Physics, 121 (2017) 203104.
[20] W. Setyawan, R.M. Gaume, S. Lam, R.S. Feigelson, S. Curtarolo, High-Throughput Combinatorial Database of Electronic Band Structures for Inorganic Scintillator Materials, ACS Combinatorial Science, 13 (2011) 382-390.
[21] Z. Jiang, A. Ramanathan, D.P. Shoemaker, In situ identification of kinetic factors that expedite inorganic crystal formation and discovery, Journal of Materials Chemistry C, 5 (2017) 5709-5717.
[22] R. Wang, D. Zhang, C. Liu, Theoretical study of silicon–oxygen–sulfur oligomers (SiOS)n (n=1–6), Chemical Physics Letters, 404 (2005) 237-243.
[23] M.S. Chandrasekharaiah, J.L. Margrave, Enthalpies of Formation of Solid Silicon Dichalcogenides, Journal of Physical and Chemical Reference Data, 23 (1994) 499-507.
[24] J.K. Larsen, S.-Y. Li, J.J.S. Scragg, Y. Ren, C. Hägglund, M.D. Heinemann, S. Kretzschmar, T. Unold, C. Platzer-Björkman, Interference effects in photoluminescence spectra of Cu2ZnSnS4 and Cu(In,Ga)Se2 thin films, Journal of Applied Physics, 118 (2015) 035307.
[25] T. Dhandayuthapani, M. Girish, R. Sivakumar, C. Sanjeeviraja, R. Gopalakrishnan, Tuning the morphology of metastable MnS films by simple chemical bath deposition technique, Applied Surface Science, 353 (2015) 449-458.
[26] S.A. Mayén-Hernández, S. Jiménez-Sandoval, R. Castanedo-Pérez, G. Torres-Delgado, B.S. Chao, O. Jiménez-Sandoval, Preparation and characterization of polycrystalline MnS thin films by

the RF-sputtering technique above room temperature, Journal of Crystal Growth, 256 (2003) 12-19.
[27] G. Vijay Kumar, V. Kanchana, G. Vaitheeswaran, Predicted thermoelectric properties of olivine-type Fe 2 GeCh 4 (Ch = S, Se and Te), Journal of Physics: Condensed Matter, 28 (2016) 025502.
[28] R. Chen, C. Persson, High absorption coefficients of the CuSb(Se,Te)2 and CuBi(S,Se)2 alloys enable high-efficient 100 nm thin-film photovoltaics, EPJ Photovolt., 8 (2017) 85504.
[29] A. Crovetto, R. Chen, R.B. Ettlinger, A.C. Cazzaniga, J. Schou, C. Persson, O. Hansen, Dielectric function and double absorption onset of monoclinic Cu2SnS3: Origin of experimental features explained by first-principles calculations, Solar Energy Materials and Solar Cells, 154 (2016) 121-129.
[30] J.J. Scragg, P.J. Dale, D. Colombara, L.M. Peter, Thermodynamic Aspects of the Synthesis of Thin-Film Materials for Solar Cells, ChemPhysChem, 13 (2012) 3035-3046.
[31] H.A.S. Platt, Copper and Iron Chalcogenides for Efficient Solar Absorption, Oregon State University, Oregon State University, Oregon State University, 2010.
[32] D.-H. Lim, P. Ramasamy, J.-S. Lee, Solution synthesis of single-crystalline Fe2GeS4 nanosheets, Materials Letters, 183 (2016) 65-68.